PCCP

PAPER

View Article Online
View Journal | View Issue

Cite this: *Phys. Chem. Chem. Phys.*, 2015, **17**, 11569

Strongly correlated plexcitonics: evolution of the Fano resonance in the presence of Kondo correlations

A. Goker

We study the optical absorption of a system consisting of a diatomic molecule that exhibits strong electron correlations coupled to metal nanoparticles possessing plasmon resonances by invoking the time-dependent non-crossing approximation. We investigate the evolution of the Fano resonance arising from the plasmon–exciton coupling when both atoms are Coulomb blockaded. We found that the Fano resonance rapidly dwindles as the ambient temperature exceeds the Kondo temperature of the singly occupied discrete state with higher energy and vanishes entirely at elevated temperatures. Our results show that even boosting the plasmon–exciton coupling above this temperature scale fails to revive the Fano resonance. We propose a microscopic model that accounts for these results. We suggest that a possible remedy for observation of the Fano resonance at high ambient temperatures is to position the singly occupied discrete state with the higher energy as close as possible to the Fermi level of the contacts while keeping the emitter resonance constant to prevent the merger of the Fano and plasmon resonances.

Received 16th February 2015,
Accepted 30th March 2015

DOI: 10.1039/c5cp00997a

www.rsc.org/pccp

1. Introduction

The ability to manipulate and control objects at the nanoscale resulting from the nanotechnology revolution[1] had profound implications in experimental studies of quantum physics, which were completely out of reach previously. This stems from the fact that the miniaturization of physical devices directly uncovers their quantum nature and the development of a suitable quantum theory is required to explain their behaviour at the nanoscale.

Designing nanoscale devices that can tailor light–matter interaction to the desired level has recently garnered tremendous attention since this tunability has the potential to pave the way for concentrating optical energy into spatial regions with dimensions less than the wavelength of illumination.[2] Collective excitation in metals called plasmons provide the means towards this end by acting as a lens. The field enhancements by these plasmon resonances that occur in confined nanostructures like metal nanoparticles[3] enable coupling with nearby quantum impurities like dots and molecules. The interaction of molecular junctions with light provides an ideal venue to study and tune these coupling reactions.[4] Coupling of the plasmons to the molecular excitation called excitons has recently been dubbed as plexcitonics.[5] This mechanism is regarded as a promising path towards realizing tunable molecular systems[6] and plasmonic switches.[7]

The classical electrodynamic simulations involving numerical solutions of Maxwell solutions fail[8,9] to capture the inherent quantum nature of interference between quasi-particles like plasmons and excitons. The observation of the Fano resonance in plexcitonics systems[10] due to the plasmon–exciton coupling mechanism further increased the need for such a quantum theory.[11] Initial attempts involving a quantum dot–metal nanoparticle system[12–14] utilized a density matrix approach to treat the oscillations of the quantum dot while the metal nanoparticles were taken to be classical. The influence of the Fano resonance on scattered photon statistics has also been reported for this system by invoking a full quantum theory.[15] All of these early treatments curtailed their realism by ignoring direct tunneling between the metal nanoparticles and the quantum dot. More recently, sophisticated methods like Zubarev's Green functions[16] and pseudoparticle nonequilibrium Green functions[17] have been invoked to explore the evolution of the Fano resonance for a single molecule[18,19] and a molecular dimer[19] attached to metal nanospheres.

However, none of these previous investigations took into account the electron spin explicitly and it is our aim in the present work to address this shortcoming. We will study a Coulomb blockaded single diatomic molecule coupled to metallic nanoparticles. We will consider each atom of the molecule to be composed of a single spin degenerate discrete level whose double occupancy by two electrons of opposite spins is prevented by the strong Coulomb repulsion occurring naturally due to the confined geometry. In particular, we will be concerned with the role of an intricate many body phenomenon called the Kondo effect on the formation of the Fano resonance in the absorption spectrum. We will show that the cotunneling events that give rise to the Kondo resonance can turn on and off the formation

Department of Physics, Bilecik University, 11210, Gülümbe, Bilecik, Turkey. E-mail: aihsan.goker@bilecik.edu.tr

of plasmon–exciton coupling. This results in the emergence and disappearance of the Fano resonance in the absorption spectrum. Our results should have direct relevance to the experiments conducted at low temperatures.

2. Theory

An excitonic diatomic molecule coupled to metal nanoparticles supporting plasmon resonances can be described with a Hamiltonian which can be explicitly written as

$$\begin{aligned} H &= \sum_{K\in\{L,R\},\sigma} \varepsilon_{K\sigma} c^{\dagger}_{K\sigma} c_{K\sigma} + \sum_{s\in\{g,e\},\sigma} \varepsilon_{s} c^{\dagger}_{s\sigma} c_{s\sigma} \\ &+ \sum_{\alpha} \varepsilon_{\alpha} a^{\dagger}_{\alpha} a_{\alpha} + \sum_{K\in\{L,R\},\sigma} \left(V_{K,g(e)} c^{\dagger}_{K\sigma} c_{g(e)\sigma} + \text{h.c.} \right) \\ &+ \sum_{K\in\{L,R\}} \varepsilon_{pK} b^{\dagger}_{K} b_{K} + J \sum_{\sigma} \left(c^{\dagger}_{g\sigma} c_{e\sigma} + \text{h.c.} \right) \\ &+ \sum_{K\in\{L,R\},\alpha} \left(W_{\alpha,K} a^{\dagger}_{\alpha} b_{K} + \text{h.c.} \right) + \frac{U}{2} \sum_{s\in\{g,e\}} n_{s\sigma} n_{s\sigma'} \\ &+ \sum_{K\in\{L,R\},\sigma} \left(\Delta_{K} c^{\dagger}_{e\sigma} c_{g\sigma} b_{K} + \text{h.c.} \right), \end{aligned} \tag{1}$$

where $c^{\dagger}_{K\sigma}(c_{K\sigma})$ and $c^{\dagger}_{s\sigma}(c_{s\sigma})$ create (annihilate) an electron with spin σ in the metal nanoparticles and in the spin degenerate discrete state of each atom within the molecule respectively. We denote these spin degenerate levels with $|g\rangle$ and $|e\rangle$ whose energy difference is $|\varepsilon_e - \varepsilon_g|$. ε_α is the energy of the radiation field with mode α and ε_{pK} is the dipolar plasmon energy in left ($K = L$) and right ($K = R$) metal nanoparticles. J and $V_{K,g(e)}$ are the electron tunneling amplitudes between the states $|g\rangle$ and $|e\rangle$ and between the metal nanoparticles and the state $|s \in \{g,e\}\rangle$, respectively. Furthermore, $W_{\alpha,K}$ and Δ_K denote the amplitudes of coupling between the radiation field with mode α and the dipolar plasmons of each nanoparticle and between the exciton within the molecule and the same dipolar plasmon modes. Finally, the U term represents the Coulomb repulsion energy within the discrete states $|g\rangle$ and $|e\rangle$ with $n_{s\sigma}$ denoting the number operator. In this work, we will ignore the contribution of the quadrupolar plasmon modes since it has been shown previously that their presence does not alter the formation and evolution of the Fano resonance that we will explore.[19]

Due to the short-range nature of the Coulomb interaction within each atom, the U term in the Hamiltonian is much larger than the other energy scales in this model. It also overwhelms the thermal energy scale in the temperature range where the Kondo correlations prevail. Consequently, we can assume that $U \to \infty$. In order to tackle this situation we perform the slave boson transformation. This procedure involves writing the electron operators acting on the states $|g\rangle$ and $|e\rangle$ in terms of a pseudofermion and a massless boson as

$$\begin{aligned} c_{g(e)\sigma} &= b^{\dagger}_{g(e)} f_{g(e)\sigma} \\ c_{g(e)\sigma} &= f^{\dagger}_{g(e)\sigma} b_{g(e)}, \end{aligned} \tag{2}$$

satisfying the condition that

$$Q_{B,g(e)} = b^{\dagger}_{g(e)} b_{g(e)} + \sum_{\sigma} f^{\dagger}_{g(e)\sigma} f_{g(e)\sigma} = 1. \tag{3}$$

The last condition is introduced to restrict the occupancy of $|g\rangle$ and $|e\rangle$ to unity. We can discard the U term and rewrite the transformed Hamiltonian as

$$\begin{aligned} H &= \sum_{K\in\{L,R\},\sigma} \varepsilon_{K\sigma} c^{\dagger}_{K\sigma} c_{K\sigma} + \sum_{s\in\{g,e\},\sigma} \varepsilon_{s} f^{\dagger}_{s\sigma} f_{s\sigma} \\ &+ \sum_{K\in\{L,R\},\sigma} \left(V_{K,g(e)} c^{\dagger}_{K\sigma} b^{\dagger}_{g(e)} f_{g(e)\sigma} + \text{h.c.} \right) \\ &+ \sum_{K\in\{L,R\}} \varepsilon_{pK} b^{\dagger}_{K} b_{K} + J \sum_{\sigma} \left(f^{\dagger}_{g\sigma} b_{g} f_{e\sigma} b^{\dagger}_{e} + \text{h.c.} \right) \\ &+ \sum_{\alpha} \varepsilon_{\alpha} a^{\dagger}_{\alpha} a_{\alpha} + \sum_{K\in\{L,R\},\alpha} \left(W_{\alpha,K} a^{\dagger}_{\alpha} b_{K} + \text{h.c.} \right) \\ &+ \sum_{K\in\{L,R\},\sigma} \left(\Delta_{K} f^{\dagger}_{e\sigma} b_{e} f_{g\sigma} b^{\dagger}_{g} b_{K} + \text{h.c.} \right) \end{aligned} \tag{4}$$

The Green function of the dipolar plasmon mode is given by

$$P(\tau,\tau') = -i \langle T_c D(\tau) D^{\dagger}(\tau) \rangle \tag{5}$$

where $D(\tau) = b_L(\tau) + b_R(\tau)$ and T_c is the contour ordering operator acting along contour c in the complex plane which we consider as the Kadanoff–Baym contour. We obtain the physical real-time correlation function $P(t,t')$ by analytical continuation using an approach introduced by Langreth.[20]

The particular choice of $D(t)$ necessitates the absorption of the photons of the incident laser in the same phase by the metal nanoparticles and it is justified if the incident laser is perpendicular to the axis connecting the metal nanoparticles. Moreover, we assume that the system is pumped by a single laser mode ε_0 which is only directly coupled to the dipolar mode. Since the molecule cannot absorb energy from the laser in this case, the J term in the Hamiltonian will be considered as zero. Based on these assumptions, we will consider the dipolar plasmon energy of each metal nanoparticle to be equal to $\varepsilon_{pL} = \varepsilon_{pR} = \varepsilon_p$. By the same token, we will be involved with only symmetrical plasmon–exciton and plasmon–laser couplings, yielding $\Delta_L = \Delta_R = \Delta$ and $W_{0,L} = W_{0,R} = W_0$ respectively in line with the previous work.[18,19]

The Dyson equations for the retarded and less than projections of the plasmon Green function can be written as

$$\left[i\frac{\partial}{\partial t} - \varepsilon_p \right] P^{r}(t,t') = \delta(t-t') + \int_{-\infty}^{\infty} \mathrm{d}t_1 \xi^{r}(t,t_1) P^{r}(t_1,t') \tag{6}$$

and

$$\begin{aligned} \left[i\frac{\partial}{\partial t} - \varepsilon_p \right] P^{>}(t,t') &= \int_{-\infty}^{\infty} (\mathrm{d}t_1 (\xi^{r}(t,t_1) P^{>}(t_1,t')) \\ &+ \xi^{>}(t,t_1) P^{a}(t_1,t')), \end{aligned} \tag{7}$$

where ε_p represents the dipolar plasmon energy. $P^{r(a)}(t,t')$ and $P^{>}(t,t')$ are the retarded (advanced) and the greater than projections

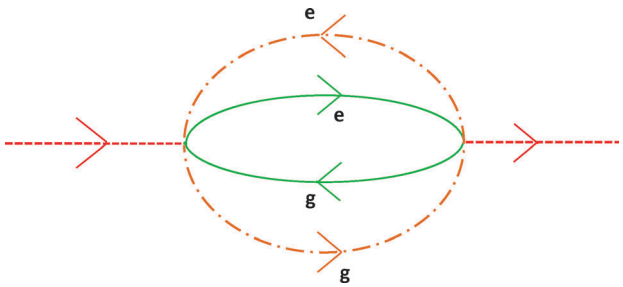

Fig. 1 Self energy of the plasmon propagator arising due to the plasmon–exciton coupling. Red (dashed) lines represent the plasmon propagator, whereas orange (dot-dashed) and green (solid) lines denote the slave boson and the pseudofermion propagators for the atom shown in the label respectively.

of the plasmon Green function. The missing ingredient to solve these Dyson equations is the plasmon self energy $\xi(t,t')$. We will resort to the non-crossing approximation to obtain the self energy.

The self energy of the plasmon due to the plasmon–exciton coupling is shown in Fig. 1. Based on this diagram, the less than and greater than projections are given by

$$\xi^{<}_{\mathrm{pe}}(t,t') = |\Delta|^2 G^{<}_{\mathrm{e}}(t,t') B^{<}_{\mathrm{g}}(t,t') G^{>}_{\mathrm{g}}(t,t') G^{>}_{\mathrm{e}}(t,t') \tag{8}$$

and

$$\xi^{>}_{\mathrm{pe}}(t,t') = |\Delta|^2 G^{>}_{\mathrm{e}}(t,t') B^{>}_{\mathrm{g}}(t,t') G^{<}_{\mathrm{g}}(t,t') G^{<}_{\mathrm{e}}(t,t'). \tag{9}$$

In order to obtain the retarded projection of the self energy, we utilize

$$\xi^{r}_{\mathrm{pe}}(t,t') = -i\Theta(t-t')\{\xi^{>}(t,t') - \xi^{<}(t,t')\}. \tag{10}$$

After some tedious algebra, the retarded self energy turns out to be

$$\begin{aligned}\xi^{r}_{\mathrm{pe}}(t,t') = {} & [G^{>}_{\mathrm{e}}(t,t') B^{r}_{\mathrm{g}}(t,t') G^{<}_{\mathrm{g}}(t,t') B^{<}_{\mathrm{e}}(t',t)] \\ & - G^{r}_{\mathrm{e}}(t,t') B^{<}_{\mathrm{g}}(t,t') G^{>}_{\mathrm{g}}(t',t) B^{>}_{\mathrm{e}}(t',t) \\ & + G^{>}_{\mathrm{e}}(t,t') B^{<}_{\mathrm{g}}(t,t') G^{<}_{\mathrm{g}}(t',t) B^{a}_{\mathrm{e}}(t',t) \\ & - G^{>}_{\mathrm{e}}(t,t') B^{<}_{\mathrm{g}}(t,t') G^{a}_{\mathrm{g}}(t',t) B^{>}_{\mathrm{e}}(t',t).\end{aligned} \tag{11}$$

On the other hand, the less than and greater than projections of the plasmon self energy due to the plasmon–laser coupling are

$$\xi^{<}_{\mathrm{pl}}(t,t') = W_0^{*}(t) D^{<}(t-t') W_0(t') \tag{12}$$

and

$$\xi^{>}_{\mathrm{pl}}(t,t') = W_0^{*}(t) D^{>}(t-t') W_0(t') \tag{13}$$

respectively. In these expressions, $D^{<}(t-t')$ is the Fourier transform of the laser induced mode population $D^{<}(\varepsilon)$ and is given by

$$D^{<}(\varepsilon) = N(\varepsilon) = \frac{1}{\pi}\frac{\delta^2}{(\varepsilon-\varepsilon_0)^2+\delta^2}, \tag{14}$$

where δ is the laser bandwidth and $D^{>}(t-t') = \delta(t-t') + D^{<}(t-t')$. Consequently, the retarded projection of the self energy due to the plasmon–laser coupling turns out to be

$$\begin{aligned}\xi^{r}_{\mathrm{pl}}(t,t') &= -i\Theta(t-t')\left\{\xi^{>}_{\mathrm{pl}}(t,t') - \xi^{<}_{\mathrm{pl}}(t,t')\right\} \\ &= -i\Theta(t-t') W_0^{*}(t)(D^{>}(t-t') - D^{<}(t-t')) W_0(t') \\ &= -i\Theta(t-t') W_0^{*}(t) W_0(t') \delta(t-t')\end{aligned} \tag{15}$$

We will now simplify our calculations by introducing

$$B^{r}_{\mathrm{g(e)}}(t,t') = -i\Theta(t-t')[B^{>}_{\mathrm{g(e)}}(t,t') - B^{<}_{\mathrm{g(e)}}(t,t')] := -i\Theta(t-t') b_{\mathrm{g(e)}}(t,t') \tag{16}$$

for the slave boson retarded Green functions. This leaves us with

$$B^{>}_{\mathrm{g(e)}}(t,t') = b_{\mathrm{g(e)}}(t,t') + B^{<}_{\mathrm{g(e)}}(t,t'). \tag{17}$$

We can repeat the same procedure for the pseudofermion retarded Green functions such that

$$G^{r}_{\mathrm{g}(r)}(t,t') = -i\Theta(t-t')[G^{>}_{\mathrm{g(e)}}(t,t') + G^{<}_{\mathrm{g(e)}}(t,t')] := -i\Theta(t-t') g_{\mathrm{g(e)}}(t,t'). \tag{18}$$

which results in

$$G^{>}_{\mathrm{g(e)}}(t,t') = g_{\mathrm{g(e)}}(t,t') - G^{<}_{\mathrm{g(e)}}(t,t'). \tag{19}$$

Using the same notation, we can rewrite the plasmon Green functions as

$$\begin{aligned}P^{r}(t,t') &= -i\Theta(t-t') p(t,t') \\ P^{a}(t,t') &= i\Theta(t'-t) p(t,t').\end{aligned} \tag{20}$$

We can now insert the self energies we obtained and the redefined Green functions into the Dyson equations. Ignoring any explicit time dependency of the plasmon–laser coupling we end up with

$$\begin{aligned}\left[\frac{\partial}{\partial t} + i\varepsilon_{\mathrm{p}}\right] p(t,t') = {} & -\int_{t'}^{t} \mathrm{d}t_1 |\Delta|^2 b_{\mathrm{g}}(t,t_1) \times (g_{\mathrm{e}}(t,t_1) \\ & - \tilde{G}^{<}_{\mathrm{e}}(t,t_1)) \tilde{G}^{<}_{\mathrm{g}}(t,t_1) \tilde{B}^{<}_{\mathrm{e}}(t_1,t) p(t_1,t') \\ & + \int_{t'}^{t} \mathrm{d}t_1 |\Delta|^2 g_{\mathrm{e}}(t,t_1)\big(g_{\mathrm{g}}(t_1,t) \\ & - \tilde{G}^{<}_{\mathrm{g}}(t_1,t)\big) \tilde{B}^{<}_{\mathrm{g}}(t,t_1)(b_{\mathrm{e}}(t_1,t) \\ & + \tilde{B}^{<}_{\mathrm{e}}(t_1,t)) p(t_1,t') + \int_{t'}^{t} \mathrm{d}t_1 |\Delta|^2 (g_{\mathrm{e}}(t,t_1) \\ & - \tilde{G}^{<}_{\mathrm{e}}(t,t_1)) \tilde{B}^{<}_{\mathrm{g}}(t,t_1) \tilde{G}^{<}_{\mathrm{g}}(t_1,t) \\ & \times b_{\mathrm{e}}^{*}(t,t_1) p(t_1,t') \\ & - \int_{t'}^{t} \mathrm{d}t_1 |\Delta|^2 \tilde{B}^{<}_{\mathrm{g}}(t,t_1)(g_{\mathrm{e}}(t,t_1) \\ & - \tilde{G}^{<}_{\mathrm{e}}(t,t_1)) g^{*}(t,t_1)(b_{\mathrm{e}}(t_1,t) \\ & + \tilde{B}^{<}_{\mathrm{e}}(t_1,t)) p(t_1,t') - |W_0|^2 p(t,t')\end{aligned} \tag{21}$$

and

$$\begin{aligned}\left[\frac{\partial}{\partial t}+i\varepsilon_p\right]P^{>}(t,t') =& -\int_{-\infty}^{t}\mathrm{d}t_1|\Delta|^2\tilde{G}_{\mathrm{g}}^{<}(t,t_1)b_{\mathrm{g}}(t,t_1)(g_{\mathrm{e}}(t,t_1)\\ &-\tilde{G}_{\mathrm{e}}^{<}(t,t_1))\tilde{B}_{\mathrm{e}}^{<}(t_1,t)P^{>}(t_1,t')\\ &+\int_{-\infty}^{t}\mathrm{d}t_1|\Delta|^2 g_{\mathrm{e}}(t,t_1)\tilde{B}_{\mathrm{g}}^{<}(t,t_1)\big(g_{\mathrm{g}}(t_1,t)\\ &-\tilde{G}_{g}^{<}(t_1,t)\big)\big(b_{\mathrm{e}}(t_1,t)+\tilde{B}_{\mathrm{e}}^{<}(t_1,t)\big)P^{>}(t_1,t')\\ &+\int_{-\infty}^{t}\mathrm{d}t_1|\Delta|^2\big(g_{\mathrm{e}}(t,t_1)-\tilde{G}_{\mathrm{e}}^{<}(t,t_1)\big)\\ &\times\tilde{B}_{\mathrm{g}}^{<}(t,t_1)\tilde{G}_{\mathrm{g}}^{<}(t_1,t)b_{\mathrm{e}}^{*}(t,t_1)P^{>}(t_1,t')\\ &-\int_{-\infty}^{t}\mathrm{d}t_1|\Delta|^2\big(g_{\mathrm{e}}(t,t_1)-\tilde{G}_{\mathrm{e}}^{<}(t,t_1)\big)\\ &\times\tilde{B}_{\mathrm{g}}^{<}(t,t_1)g_{\mathrm{g}}{}^{*}(t,t_1)(b_{\mathrm{e}}(t_1,t)\\ &+\tilde{B}_{\mathrm{e}}^{<}(t_1,t))P^{>}(t_1,t')-|W_0|^2P^{>}(t,t')\\ &+\int_{-\infty}^{t'}\mathrm{d}t_1|\Delta|^2\tilde{G}_{\mathrm{g}}^{<}(t_1,t)\\ &\times\big(g_{\mathrm{e}}(t,t_1)-\tilde{G}_{\mathrm{e}}^{<}(t,t_1)\big)\big(b_{\mathrm{g}}(t,t_1)\\ &+\tilde{B}_{\mathrm{g}}^{<}(t,t_1)\big)\tilde{B}_{\mathrm{e}}^{<}(t_1,t)p(t_1,t')\\ &+\int_{-\infty}^{t'}\mathrm{d}t_1|W_0|^2D^{<}(t-t_1)p(t_1,t')\\ &+|W_0|^2p(t_1,t').\end{aligned}\tag{22}$$

The retarded pseudofermion and slave boson Green functions in eqn (21) and (22) are determined by solving the relevant Dyson equations given by

$$\left[\frac{\partial}{\partial t}+i\varepsilon_{\mathrm{g(e)}}\right]g_{\mathrm{g(e)}}(t,t')=-\int_{t'}^{t}\mathrm{d}t_1K_{\mathrm{g(e)}}^{>}(t,t_1)b_{\mathrm{g(e)}}(t,t_1)g_{\mathrm{g(e)}}(t_1,t')\tag{23}$$

and

$$\frac{\partial}{\partial t}b_{\mathrm{g(e)}}(t,t')=-\int_{t'}^{t}\mathrm{d}t_1K_{\mathrm{g(e)}}^{<}(t_1,t)g_{\mathrm{g(e)}}(t,t_1)b_{\mathrm{g(e)}}(t_1,t').\tag{24}$$

In eqn (23) and (24) the pseudofermion and slave boson self energies are expressed with the aid of the diagrams shown in Fig. 2. Consequently $K_{\mathrm{g(e)}}^{>}(t,t')$ and $K_{\mathrm{g(e)}}^{<}(t,t')$ are written as

$$\begin{aligned}K_{\mathrm{g(e)}}^{<}(t,t') &= \bar{\Gamma}\int_{-D}^{D}\frac{\mathrm{d}\varepsilon}{2\pi}\rho(\varepsilon)\frac{1}{1+\mathrm{e}^{\beta\varepsilon}}\mathrm{e}^{i\varepsilon(t-t')}\\ K_{\mathrm{g(e)}}^{>}(t,t') &= \bar{\Gamma}\int_{-D}^{D}\frac{\mathrm{d}\varepsilon}{2\pi}\rho(\varepsilon)\frac{\mathrm{e}^{\beta\varepsilon}}{1+\mathrm{e}^{\beta\varepsilon}}\mathrm{e}^{i\varepsilon(t-t')},\end{aligned}\tag{25}$$

where $\rho(\varepsilon)$ represents the density of states of the metal nanoparticles with a half bandwidth of D and $\bar{\Gamma}=2\pi|V_{K,\mathrm{g(e)}}(\varepsilon_f)|^2$. In this expression, ε_f denotes the Fermi level of the metal nanoparticles. We ignore any explicit time and energy dependence of the tunneling matrix elements and consider $V_{K,\mathrm{g(e)}}(\varepsilon)=V_{K,\mathrm{g(e)}}(\varepsilon_f)$. We will consider a symmetrically coupled molecule in this paper where $V_{L,\mathrm{g(e)}}=V_{R,\mathrm{g(e)}}$. Furthermore, we assume that the coupling of each atom to the nanoparticles is equal implying that $V_{K,g}=V_{K,\mathrm{e}}$. We also define $\Gamma(\varepsilon)=\bar{\Gamma}\rho(\varepsilon)$ and consider Γ as the value of $\Gamma(\varepsilon)$ at ε_f. Left and right nanoparticles are assumed to be identical and hence their density of states is the same. For simplicity, we will use parabolic density of states with $D=9\Gamma$ in our calculations. In principle, we have the capability of taking into account the realistic band structure of the metal nanoparticles.[21–23] However, this requires an extra *ab initio* calculation and it is beyond our scope in this paper.

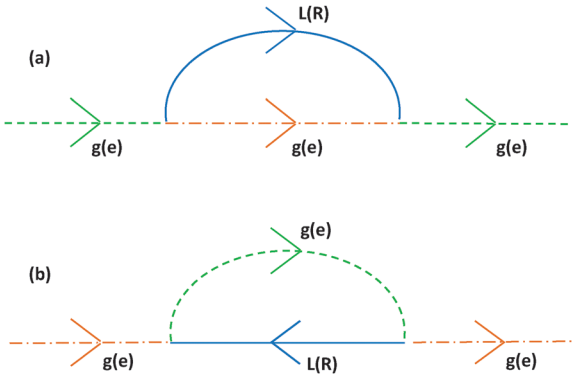

Fig. 2 Panels (a) and (b) illustrate the self energy of each atom's pseudofermion and the slave boson propagator respectively due to the molecule–nanoparticle coupling. Green (dashed) lines represent the pseudofermion propagator, whereas orange (dot-dashed) and blue (solid) lines denote the slave boson propagator for the same atom and the electron propagator in the nanoparticle to which the pseudofermion tunnels, respectively.

After obtaining the retarded pseudofermion and slave boson Green functions in this manner, the less than projections of these Green functions can be obtained by solving

$$\begin{aligned}\left[\frac{\partial}{\partial t}+i\varepsilon_{\mathrm{g(e)}}\right]G_{\mathrm{g(e)}}^{<}(t,t') &= \int_{-\infty}^{t'}\mathrm{d}t_1K_{\mathrm{g(e)}}^{<}(t,t_1)B_{\mathrm{g(e)}}^{<}(t,t_1)g_{\mathrm{g(e)}}(t_1,t')\\ &-\int_{-\infty}^{t}\mathrm{d}t_1K_{\mathrm{g(e)}}^{>}(t,t_1)b_{\mathrm{g(e)}}(t,t_1)G_{\mathrm{g(e)}}^{<}(t_1,t')\end{aligned}\tag{26}$$

and

$$\begin{aligned}\frac{\partial}{\partial t}B_{\mathrm{g(e)}}^{<}(t,t') &= \int_{-\infty}^{t'}\mathrm{d}t_1K_{\mathrm{g(e)}}^{>}(t_1,t)G_{\mathrm{g(e)}}^{<}(t,t_1)b_{\mathrm{g(e)}}(t_1,t')\\ &-\int_{-\infty}^{t}\mathrm{d}t_1K_{\mathrm{g(e)}}^{<}(t_1,t)g_{\mathrm{g(e)}}(t,t_1)B_{\mathrm{g(e)}}^{<}(t_1,t').\end{aligned}\tag{27}$$

The values of all Green functions are stored in a square matrix. The details of the discretization and numerical solution of the Dyson equations have been reported in detail previously.[24,25] We insert the values of pseudofermion and slave boson Green functions into eqn (21) and (22) to obtain the plasmon Green functions. The matrix size of the plasmon Green function is chosen to be the same as the pseudofermion and slave boson Green functions. The matrix size is gradually increased and the

matrix is propagated along the diagonal direction to achieve convergence.

When the discrete energy levels ε_g and ε_e lie below the Fermi level of the metal nanoparticles ε_f, the density of states of each discrete level at sufficiently low temperatures exhibits two distinct features. One of them is a broad resonance with a linewidth Γ centered around each discrete level. This resonance is called the Breit–Wigner resonance and originates from the hybridization of the discrete levels with the metal nanoparticles. Therefore, it is a noninteracting phenomenon and will exist even in the absence of any Coulomb interactions. The second feature is a quite sharp resonance situated slightly above the Fermi level of the metal nanoparticles ε_f with a linewidth on the order of

$$T_{K,g(e)} \propto \left(\frac{D\Gamma}{4}\right)^{\frac{1}{2}} \exp\left(-\frac{\pi\left|\varepsilon_{g(e)}\right|}{\Gamma}\right). \tag{28}$$

This resonance is called the Kondo resonance and its linewidth, which is an energy scale, is the Kondo temperature. The formation of the Kondo resonance is related to the cotunneling processes at ambient temperatures below $T_{K,g(e)}$ where two electrons with different spins tunnel simultaneously giving rise to an effective spin flip at the discrete levels. The Kondo resonance is an elegant trademark of the many body physics and it is completely absent in the noninteracting limit.

A crucial point while inserting the pseudofermion and slave boson Green functions into eqn (21) and (22) is that we obtain the less than Green functions in the wide band limit and plug those values into the Dyson equations. This means they do not incorporate a Kondo resonance and correspond to the noninteracting limit. These Green functions are denoted by a tilde on top to differentiate them from the interacting retarded ones.

Despite its seemingly drastic nature, this is not an additional approximation and is required because of the projection into the $Q_{B,g(e)} = 1$ subspace. The underlying reason is the $Q_{B,g(e)}$ dependency of the various Green functions. The retarded and less than plasmon Green functions are of the order $Q^0_{B,g(e)}$. Consequently, the self energies multiplying them in Dyson equations must be of the order $Q^0_{B,g(e)}$ too. The retarded pseudofermion and slave boson Green functions are of the order $Q^0_{B,g(e)}$ while the less than ones are of the order $Q^1_{B,g(e)}$. In order to maintain $Q^0_{B,g(e)}$ dependency on both sides of eqn (21) and (22), we calculate the less than pseudofermion and retarded Green functions in the wide band limit which amounts to the noninteracting limit and renders them on the order of $Q^0_{B,g(e)}$. Eqn (21) and (22) are the main results of this paper and we will explore their ramifications for the optical absorption of the system in the next section.

3. Results and discussion

Optical absorption in the steady state for the laser energy ε_0 is given by[19]

$$I_{\mathrm{abs}}(\varepsilon_0) = -\int_0^\infty \frac{\mathrm{d}\varepsilon}{2\pi}\gamma(\varepsilon)N(\varepsilon)\mathrm{Im}P^{>}(\varepsilon), \tag{29}$$

where the total plasmon dissipation rate is defined as

$$\gamma(\varepsilon) = 2\pi \sum_{K\in\{L,R\}} \left|W_{0,K}\right|^2 \delta(\varepsilon - \varepsilon_0), \tag{30}$$

with $N(\varepsilon)$ being the laser induced mode population in eqn (14) and $P^{>}(\varepsilon)$ the Fourier transform of the greater than plasmon Green function $P^{>}(t,t')$.

We consider the dipolar plasmon energy ε_p = 3.49 eV, the laser bandwidth δ = 1 meV and coupling of the dipolar plasmon to the laser $\gamma_{L(R)} = 2\pi\left|W_{0,L(R)}\right|^2$ = 86 meV in conjunction with the previous studies.[18,19] Moreover, we will keep the coupling of the electrons to the contacts constant by taking $\bar{\Gamma}$ = 0.2 eV and Γ = 0.8 eV.

We start by calculating the optical absorption spectrum of a system where the singly occupied discrete energy levels are considered to be $\varepsilon_g = -4.8$ eV and $\varepsilon_e = -1.6$ eV. This results in an emitter resonance energy of 3.2 eV which is equal to the energy gap between the discrete states. The plasmon–exciton coupling is initially kept as a fixed parameter with $\Delta_{L(R)}$ = 20 meV in line with earlier work.[18,19]

The optical absorption spectrum of a metal nanoparticle dimer–molecule system for various ambient temperatures is shown in Fig. 3. There are two prominent features of this spectrum. One of them is the dipole plasmon resonance centered around ε_p. The other is the Fano resonance located around the emitter energy. We would like to note that the quadrupole plasmon mode would also appear as a shoulder on the right-hand side of the dipole plasmon;[18] however, we ignore it in this work because it has been shown that its presence does not affect the formation of the Fano resonance.[19]

The most striking highlight of Fig. 3 is the temperature sensitivity of the Fano resonance. It is quite robust below 20 K. However, it starts to shrink as the temperature is increased above this value and it almost vanishes completely above 40 K. On the other hand, the plasmon resonance appears to be quite resilient during this transition and it stays intact at any temperature.

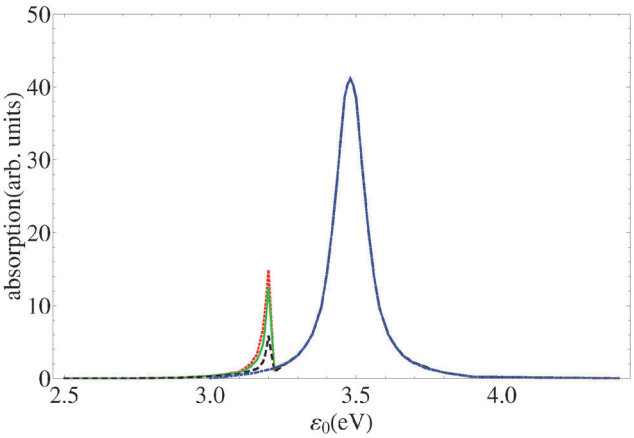

Fig. 3 The optical absorption spectrum of the molecule–metal nanoparticle dimer system as a function of the incident laser energy ε_0 with $\varepsilon_g = -4.8$ eV and $\varepsilon_e = -1.6$ eV at ambient temperatures of T = 12 K (red dotted), T = 24 K (purple solid), T = 36 K (black dashed) and T = 48 K (blue dot-dashed) respectively assuming a plasmon–exciton coupling of Δ = 20 meV.

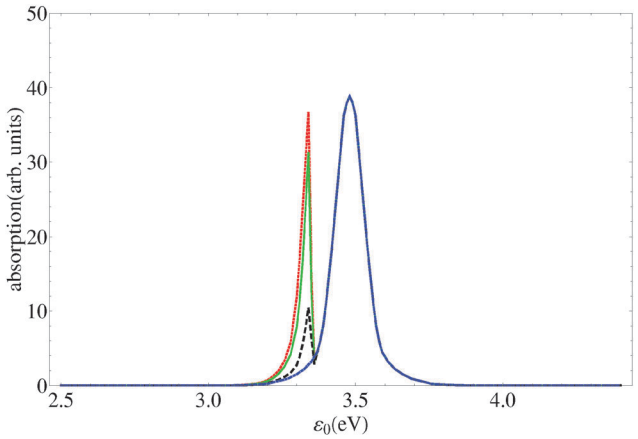

Fig. 4 The optical absorption spectrum of the molecule–metal nanoparticle dimer system as a function of the incident laser energy ε_0 with $\varepsilon_g = -4.95$ eV and $\varepsilon_e = -1.6$ eV at ambient temperatures of $T = 12$ K (red dotted), $T = 24$ K (purple solid), $T = 36$ K (black dashed) and $T = 48$ K (blue dot-dashed) respectively assuming a plasmon–exciton coupling of $\Delta = 20$ meV.

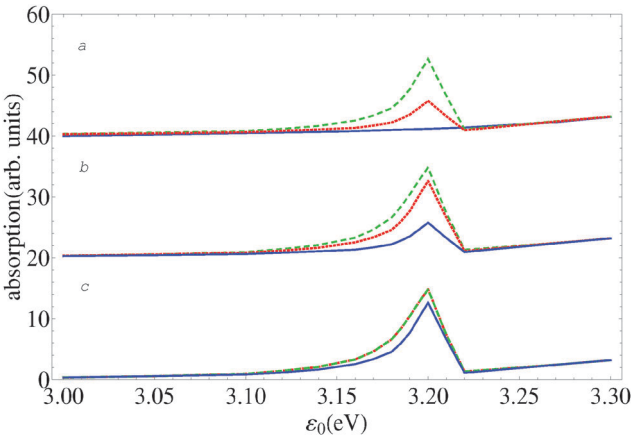

Fig. 5 The optical absorption spectrum of the molecule–metal nanoparticle dimer system as a function of the incident laser energy ε_0 for system 1 (green dashed), system 2 (red dotted) and system 3 (blue solid) as described in the text at $T = 24$ K (panel a), $T = 12$ K (panel b) and $T = 6$ K (panel c) assuming a plasmon–exciton coupling of $\Delta = 20$ meV. The curves in panels a and b have been shifted upwards to enable comparison at the same ambient temperature values.

The Kondo temperature of ε_e turns out to be about 23 K according to eqn (28) whereas the Kondo temperature of ε_g is zero for all practical purposes.

We then calculate the optical absorption spectrum of the same molecule–metal nanoparticle dimer system with the same parameters in Fig. 3 except that we consider $\varepsilon_g = -4.95$ eV this time. The results are shown in Fig. 4. The plasmon resonance is again located around the dipole plasmon energy and quite robust against a temperature sweep. On the other hand, the Fano resonance shifts to a slightly higher energy since the emitter resonance energy increased in this case. Despite this, we observe that the same temperature sensitivity prevails here too. Even though the Fano resonance is fully formed below 20 K, it starts to diminish once the temperature is increased above this and disappears when it exceeds 40 K just like the previous situation. This implies that the value of ε_g has hardly any influence on this bevahivour of the Fano resonance.

We now want to explore the influence of tuning the value of ε_e on the development of the Fano resonance. Towards this end, we choose three different molecule–metal nanoparticle dimer systems which have the same emitter resonance energy. This enables a direct comparison since each system has a different ε_e. We will refer to the configurations where $\varepsilon_e = -1.6$ eV and $\varepsilon_g = -4.8$ eV as system 1, $\varepsilon_e = -1.8$ eV and $\varepsilon_g = -5.0$ eV as system 2, $\varepsilon_e = -2.0$ eV and $\varepsilon_g = -5.2$ eV as system 3 in the following discussion. The results for all these sytems at various ambient temperatures are shown in Fig. 5. Only the close vicinity of the Fano resonance is displayed here since the plasmon resonance has been found to be insensitive to temperature fluctuations above.

First of all, the Fano resonance is located around the same energy value for all three systems due to the equivalence of the emitter resonance energy. However, this is where the similarity ends and we see that the Fano resonance behaves differently for all the systems studied. The Fano resonance of system 1, where the Kondo temperature of ε_e is around 23 K, turns out to be the most resilient against increasing temperature. On the other hand, the Fano resonance of system 2 is significantly inhibited at 24 K and vanishes at higher temperatures. We estimate that the Kondo temperature of ε_e is around 11 K for this system. The Fano resonance of system 3 turns out to be the least resilient against ramped up temperature. It dwindles even at 12 K and it is completely wiped off at 24 K and any temperature above it. The Kondo temperature of ε_e is estimated to be around 5 K for system 3.

These results suggest that the Kondo temperature of ε_e is a critical parameter that determines the survival of the Fano resonance of the molecule–metal nanoparticle dimer system when the ambient temperature increases. A higher Kondo temperature for ε_e by positioning it closer to the Fermi level of the metal nanoparticles ensures that the Fano resonance can stay intact at elevated temperatures.

We finally want to investigate whether elevating the plasmon–exciton coupling can mitigate inhibition of the Fano resonance at temperatures above the Kondo temperature of ε_e. Towards this end, we revisited the system shown in Fig. 4 and calculated the optical absorption spectrum by increasing the plasmon–exciton coupling value to $\Delta = 40$ meV. The results are shown in Fig. 6. At first glance, one can notice that this results in a deeper trough between the Fano resonance and the plasmon resonance causing a more pronounced separation between these two peaks in line with earlier results.[18] Apart from this obvious fact, we still witness the gradual collapse of the Fano resonance with increasing ambient temperature leading to its eventual disappearance at temperatures significantly above the Kondo temperature of ε_e just like in Fig. 4. This means that even elevated plasmon–exciton coupling values fail to ensure the survival of the Fano resonance and its formation is somehow intrinsically linked to the existence of the Kondo resonance around ε_e.

Finally, we would like to present a microscopic scenario which provides a tangible explanation for our results in this paper. The emergence of the Fano resonance in the optical absorption

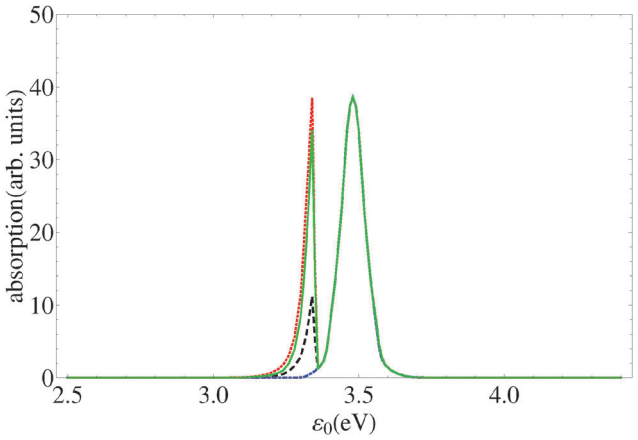

Fig. 6 The optical absorption spectrum of the molecule–metal nanoparticle dimer system as a function of the incident laser energy ε_0 with $\varepsilon_g = -4.95$ eV and $\varepsilon_e = -1.6$ eV at ambient temperatures of $T = 12$ K (red dotted), $T = 24$ K (purple solid), $T = 36$ K (black dashed) and $T = 48$ K (blue dot-dashed) respectively assuming a plasmon–exciton coupling of $\Delta = 40$ meV.

spectrum is enabled by the plasmon–exciton coupling which requires the tunneling of an electron residing in $|g\rangle$ to $|e\rangle$ when the plasmon is destroyed in one of the metallic nanoparticles or *vice versa*. However, this process is not allowed in the sequential tunneling regime since the double occupancy of either discrete state is forbidden. Therefore, the Fano resonance gets rapidly suppressed above $T_{K,e}$. Once the ambient temperature is reduced below this scale, cotunneling events start taking place at $|e\rangle$, whereby the electron occupying this level can tunnel into one of the metal nanoparticles leaving it empty momentarily. This breaks the blockade of plasmon–exciton coupling and another electron with opposite spin occupying $|g\rangle$ can tunnel to $|e\rangle$. This gives rise to an effective spin flip process at $|e\rangle$ producing a sharp Kondo resonance in its density of states. Consequently, a Fano resonance develops in the optical absorption spectrum in tandem. The reverse electron transport process takes place when the plasmon is created again. Since the laser is only coupled to the metallic nanoparticles, the plasmon resonance has no temperature dependency.

A major drawback of our results is that one may need to go to quite low ambient temperatures in a strongly correlated system to be able to observe the Fano resonance in the absorption spectrum. The simplest way of circumventing this problem is to study a system which is not Coulomb blockaded. In such a system, the plasmon–exciton coupling can take place at any ambient temperature because an electron can sequentially tunnel between the discrete states that can be doubly occupied. Therefore, it is possible to observe the Fano resonance even at room temperature in that case. However, the only way of overcoming this hurdle in a Coulomb blockaded system that we considered here is to increase the value of $T_{K,e}$ by shifting $|e\rangle$ towards the Fermi level of the metallic nanoparticles as much as possible. The adverse affect of performing this would be a possible merger of the Fano resonance with the plasmon resonance if $|g\rangle$ stays far away from the Fermi level. This is simply because this action would increase the emitter resonance energy by itself. Consequently, the realignment of $|e\rangle$ must be accompanied by an equal amount of upward shift of $|g\rangle$ towards the Fermi level to keep the separation between the two resonances constant. This would ensure the survival and observation of the Fano resonance in experiments performed at noncryogenic ambient temperatures.

We would also like to mention a possible complication that can arise in an experiment. The laser illumination of metal nanoparticles can lead to heat generation and therefore may prevent one from reaching low ambient temperatures below the Kondo temperature. It has been shown that this adverse effect can be overcome by using a laser whose pulse duration is much longer than 100 ps.[26] This curbs the temperature rise in the molecule–metal nanoparticle dimer system significantly by diffusing the heat to the environment.

4. Conclusion

In this paper, we developed a novel theory to account for the strong electron correlations in a molecule–metal nanoparticle dimer system which exhibits a Fano resonance in the optical absorption spectrum due to the coupling of the plasmon resonance of the metallic nanoparticles to the molecular excitons. We thoroughly investigated the evolution of the Fano resonance as a function of the ambient temperature by expressing the plasmon self energy *via* the non-crossing approximation and solving the relevant Dyson equations.

We determined unambiguously that the formation of the Fano resonance is closely linked to the development of the Kondo resonance around the singly occupied discrete state with the higher energy. This conclusion stems from the fact that the Fano resonance gets inhibited at ambient temperatures above the Kondo temperature of this state and even boosting of the plasmon–exciton coupling fails to revive it.

We proposed a microscopic scenario to explain these results based on the spin–flip processes that give rise to the formation of the Kondo resonance. We concluded that the exciton formation is blocked within the molecule without these spin–flip processes since both discrete states of the molecule are Coulomb blockaded. Consequently, we put forward a scenario where the discrete state ε_e should be positioned as close as possible to the Fermi levels of the metal nanoparticles in order to observe the Fano resonance at elevated ambient temperatures. Moreover, the emitter resonance should also be kept constant towards this end in order to prevent the merger of the Fano resonance with the plasmon resonance. We hope to motivate further experiments in this rapidly evolving field with our results.

Acknowledgements

The author thanks Tübitak for generous financial support *via* grants 111T303 and 114F195 and to Dr Hüseyin Aksu for several useful discussions.

References

1 H. W. Kroto, J. R. Heath, S. C. O'Brien, S. C. Curl and R. E. Smalley, *Nature*, 1985, **318**, 162.
2 S. A. Maier, *Plasmonics: Fundamentals and applications*, Springer, New York, 2007.
3 R. A. Alvarez Puebla, L. M. Liz-Marzan and F. J. G. de Abajo, *J. Phys. Chem. Lett.*, 2010, **1**, 2428.
4 M. Galperin and A. Nitzan, *Phys. Chem. Chem. Phys.*, 2012, **14**, 9421–9438.
5 N. T. Fofang, T. H. Park, O. Neumann, N. A. Mirin, P. Nordlander and N. J. Halas, *Nano Lett.*, 2008, **8**, 3481–3487.
6 G. A. Wurtz, P. R. Evans, W. Hendren, R. Atkinson, W. Dickson, R. J. Pollard, A. V. Zayats, W. Harrison and C. Bower, *Nano Lett.*, 2007, **7**, 1297–1303.
7 Y. B. Zheng, B. Kiraly, S. Cheunkar, T. J. Huang and P. S. Weiss, *Nano Lett.*, 2011, **11**, 2061–2065.
8 A. Coomar, C. Arntsen, K. A. Lopata, S. Pistinner and D. Neuhauser, *J. Chem. Phys.*, 2011, **135**, 084121.
9 S. Li, Y. Gao and D. Neuhauser, *J. Chem. Phys.*, 2012, **136**, 234104.
10 B. Luk'yanchuk, N. I. Zheludev, S. A. Maier, N. J. Halas, P. Nordlander, H. Giessen and C. T. Chong, *Nat. Mater.*, 2010, **9**, 707–715.
11 M. S. Tame, K. R. McEnery, S. K. Özdemir, J. Lee, S. A. Maier and M. S. Kim, *Nat. Phys.*, 2013, **9**, 329–340.
12 W. Zhang, A. O. Govorov and G. W. Bryant, *Phys. Rev. Lett.*, 2006, **97**, 146804.
13 R. D. Artuso and G. W. Bryant, *Nano Lett.*, 2008, **8**, 2106–2111.
14 R. D. Artuso and G. W. Bryant, *Phys. Rev. B: Condens. Matter Mater. Phys.*, 2010, **82**, 195419.
15 A. Ridolfo, O. D. Stefano, N. Fina, R. Saija and S. Savasta, *Phys. Rev. Lett.*, 2010, **105**, 263601.
16 D. N. Zubarev, *Sov. Phys. Usp.*, 1960, **3**, 320.
17 A. J. White and M. Galperin, *Phys. Chem. Chem. Phys.*, 2012, **14**, 13809–13819.
18 A. Manjavacas, F. J. G. de Abajo and P. Nordlander, *Nano Lett.*, 2011, **11**, 2318–2323.
19 A. J. White, B. D. Fainberg and M. Galperin, *J. Phys. Chem. Lett.*, 2012, **3**, 2738–2743.
20 D. C. Langreth, in *Linear and Nonlinear Electron Transport in Solids*, ed. J. T. Devreese and V. E. van Doren, Plenum, New York, 1976.
21 A. Goker, Z. Y. Zhu, A. Manchon and U. Schwingenschlogl, *Chem. Phys. Lett.*, 2011, **509**, 48.
22 A. Goker, Z. Y. Zhu, A. Manchon and U. Schwingenschlogl, *Phys. Rev. B: Condens. Matter Mater. Phys.*, 2010, **82**, 161304(R).
23 A. Goker, B. A. Friedman and P. Nordlander, *J. Phys.: Condens. Matter*, 2007, **19**, 376206.
24 H. X. Shao, D. C. Langreth and P. Nordlander, *Phys. Rev. B: Condens. Matter Mater. Phys.*, 1994, **49**, 13929–13947.
25 A. F. Izmaylov, A. Goker, B. A. Friedman and P. Nordlander, *J. Phys.: Condens. Matter*, 2006, **18**, 8995–9006.
26 B. S. Luk'yanchuk, A. E. Miroshnichenko, M. I. Tribelsky, Y. S. Kivshar and A. R. Khokhlov, *New J. Phys.*, 2012, **14**, 093022.

